Cryo-electron microscopy of low density lipoprotein and reconstituted discoidal high density lipoprotein: imaging of the apolipoprotein moiety

Rik van Antwerpen,[1,*] G. Chi Chen,[§] Clive R. Pullinger,[§] John P. Kane,[§] Michael LaBelle,[**] Ronald M. Krauss,[**] Cesar Luna-Chavez,[**] Trudy M. Forte,[**] and John C. Gilkey[†]

Department of Biochemistry* and Department of Pharmacology,[†] University of Arizona, Tucson, AZ 85721; Cardiovascular Research Institute,[§] Department of Medicine, University of California, San Francisco, CA 94143; and Ernest Orlando Lawrence Berkeley National Laboratory,[**] University of California, Berkeley, CA 94720

Abstract Cryo-electron microscopy was used to analyze the structure of low density lipoprotein from normolipidemic subjects (N-LDL), phospholipid-depleted N-LDL (PD-LDL), small dense LDL from hypertriglyceridemic subjects (SD-LDL), and reconstituted discoidal high density lipoproteins (rHDL). In different projections of N-LDL, a high density component of the particle was visible as two parallel bands or as a single ring. Projections of PD-LDL were very similar to those of N-LDL, indicating that the contribution of phospholipid headgroups to the observed high density structure is minor. In preparations of SD-LDL, projections with two high density bands or a single high density ring were rare. Instead, triangular and diamond-shaped projections were recognized. In different projections of discoidal rHDL, a high density component was visible as a single band or as a single ring. The present results indicate that cryo-electron microscopy reveals the distribution of apolipoproteins within lipoprotein particles. Thus, apolipoprotein B-100 (apoB) in N-LDL appears to be organized as a double ring around the particle, while apoB in SD-LDL is indicated to have a different conformation. Cryo-electron micrographs of rHDL are consistent with the presence of apolipoprotein A-I on the periphery of the lipoprotein disc.—**van Antwerpen, R., G. C. Chen, C. R. Pullinger, J. P. Kane, M. LaBelle, R. M. Krauss, C. Luna-Chavez, T. M. Forte, and J. C. Gilkey.** Cryo-electron microscopy of low density lipoprotein and reconstituted discoidal high density lipoprotein: imaging of the apolipoprotein moiety. *J. Lipid Res.* 1997. **38:** 659–669.

Supplementary key words transmission electron microscopy • cold stage • LDL • HDL • lipoprotein structure

Current models of the human low density serum lipoprotein (LDL) describe the particle as an 18–25 nm sphere with a hydrophobic core of cholesteryl esters and triacylglycerol (1). The surface of the lipoprotein is thought to consist of phospholipids, free cholesterol, and a single molecule of apolipoprotein B-100 (apoB; M_r = ca. 550,000) (1). The complete amino acid sequence of apoB has been determined and different domains, including the LDL receptor binding domain, have been identified (2–4). Negative staining electron microscopy of lipid extracted LDL (5) and immunoelectron microscopy of intact LDL (6,7) have indicated that apoB may form a "ribbon-like" structure that encircles the lipoprotein particle. On the basis of recent epitope mapping experiments, Chatterton et al. (7) have suggested that the C-terminal part of apoB in LDL may form a "bow" structure that folds back on part of the apolipoprotein molecule. The authors propose that an interaction of this bow with specific domains on the ribbon may control access to the receptor binding domain of LDL (7).

Although relatively little is known about the detailed secondary and tertiary structure of apoB in LDL, several studies have indicated that the apolipoprotein may assume different conformations in different LDL subclasses. For example, apoB in small dense LDL from hypertriglyceridemic subjects (SD-LDL) has a higher content of β-structure (8, 9) and an altered proteolytic accessibility (8) compared to apoB in LDL from normolipidemic subjects (N-LDL). In addition, SD-LDL has a decreased affinity for the LDL receptor of human fibroblasts (8, 9). An aberrant conformation of apoB in SD-LDL may well be responsible for the observed decrease in receptor binding.

Abbreviations: LDL, low density lipoprotein; N-LDL, LDL from normolipidemic subjects; PD-LDL, phospholipid-depleted N-LDL; SD-LDL, small dense LDL from hypertriglyceridemic subjects; rHDL, reconstituted high density lipoprotein.

[1]To whom correspondence should be addressed.

Recently, we have analyzed the structure of N-LDL using cryo-electron microscopy (10). The results of this study indicate that structural elements of high mass density are organized as a double ring that encircles the lipoprotein particle. As apoB is the principal high density component of LDL, our results suggest that cryo-electron microscopy visualizes the distribution of this apolipoprotein within the LDL particle. This conclusion is supported by the recent cryo-electron microscopic analysis of human LDL by Spin and Atkinson (11). However, phospholipid headgroups constitute an additional high density component of LDL (1), and earlier studies have indicated that phospholipid headgroups are depicted with positive contrast in cryo-electron micrographs of model membranes (12, 13). Hence, additional studies are needed to determine whether cryo-electron microscopy indeed visualizes the distribution of apoB in N-LDL.

In the present cryo-electron microscopic study, we compared the structural features of N-LDL and phospholipid depleted N-LDL (PD-LDL), in order to estimate the contribution of phospholipid headgroups to the high density structure that is seen in cryo-electron micrographs of N-LDL. In addition, we analyzed the structure of SD-LDL to determine whether cryo-electron microscopy can reveal the conformational difference that is thought to exist between the apoBs of N-LDL and SD-LDL. Finally, we tested the hypothesis that cryo-electron microscopy visualizes the apolipoprotein moiety of lipoprotein particles by analyzing reconstituted discoidal high density lipoproteins (rHDL), which are phospholipid bilayers that are stabilized at the edge by apolipoprotein A-I (apoA-I) (14, 15). Our observations indicate that cryo-electron microscopy indeed reveals the distribution of apolipoproteins in lipoprotein particles, and that the contribution of phospholipid headgroups to the observed high density structures is relatively minor. The data are consistent with the presence of apoA-I on the periphery of the rHDL disc, and confirm earlier indications that apoB in N-LDL is organized as a double ring around the lipoprotein particle. Furthermore, the results are consistent with the presence of a major conformational difference between the apoBs of N-LDL and SD-LDL.

MATERIALS AND METHODS

Materials

Trolox (6-hydroxy-2,5,7,8-tetramethylchroman-2-carboxylic acid) was obtained from Hoffman La Roche. Phosphorus calibrator, aminoethylbenzylsulfonyl fluoride (AEBSF), and cholesterol were from Sigma Chemical Company (St. Louis, MO). Phospholipase A_2 (from bee venom) was obtained from Boehringer Mannheim (Indianapolis, IN). Purified phospholipid 1-palmitoyl-2-linoleoyl-phosphatidylcholine (PLPC), >99% pure, was purchased from Avanti Polar Lipids, Inc. (Alabaster, AL). Copper electron microscope grids (300 mesh) with lacey substrates were from Ted Pella, Inc. (Redding, CA).

Isolation of N-LDL

Plasma samples were obtained after overnight fast from normal subjects. None of the subjects was a smoker or using drugs known to affect lipid metabolism. Blood was collected into Vacutainers containing 1 mg of EDTA per ml and 10 μM Trolox, a water-soluble vitamin E analog, and cells were pelleted by centrifugation at 2000 *g* for 30 min at 4°C. LDL was isolated by sequential ultracentrifugation (16). LDL was dialyzed into 10 mM Tris-HCl (pH 7.5), 150 mM NaCl, 1 mM EDTA, 10 μM Trolox and stored at 4°C under nitrogen.

Preparation of PD-LDL

N-LDL samples were incubated in 25 mM Tris-HCl, 150 mM NaCl, 0.25% (w/v) human serum albumin (fatty acid-free), 10 mM $CaCl_2$, 1 mM AEBSF, and 5 U of bee venom phospholipase A_2 per μg LDL protein for 3 h at 37°C. Control samples were incubated in the same buffer without enzyme. After incubation LDL was re-isolated by ultracentrifugation and the amount of phospholipid remaining after phospholipase treatment was measured using a standardized colorimetric method (17) and a phosphorus calibrator PD-LDL was determined to have ca. 79% less phospholipid than N-LDL. PD-LDL ran more slowly than N-LDL on agarose gels, due to the contribution of phospholipids to the net charge of the LDL particle, and SDS-PAGE demonstrated that the described phospholipase treatment did not fragment the apoB molecule (results not shown).

Isolation of SD-LDL

SD-LDL was isolated from the plasma of fasting hypertriglyceridemic subjects, and was determined to belong to the LDL-4.5 subclass, as described previously (8). LDL-4.5 particles are among the smallest and densest LDL particles identified [density interval 1.052–1.058 g/ml (8)].

Reconstituted discoidal HDL (rHDL)

Apolipoprotein A-I (apoA-I) was prepared by the guanidine hydrochloride method previously described (18). A single band at 28 kDa was observed on SDS-PAGE. Discoidal complexes were prepared by the sodium-cholate dialysis procedure (19) using 1-palmitoyl-

2-linoleoyl-phosphatidylcholine: cholesterol: apoA-I: Na cholate molar ratios of 150:37.5:1:270. The complexes were fractionated by gel filtration on Bio-Gel A1.5M (Bio-Rad Laboratories) and were maintained in a background buffer of 20 mM Tris, 150 mM NaCl, 0.27 mM EDTA, pH 7.4. The complex containing 4 apoA-Is per particle, as determined by chemical crosslinking with dimethylsuberimidate (20), was used for cryo-electron microscopy. Upon non-denaturing gradient gel electrophoresis (21) this complex banded at 18.2 nm.

Protein assay

Protein concentrations were determined by a modification (22) of the method of Lowry et al. using BSA as the standard.

Electron microscopy

Lipoprotein samples were analyzed by negative staining according to Forte and Nordhausen (23). Size measurements of particles in negatively stained preparations were performed on free standing particles with a circular profile. Average dimensions, plus and minus standard deviation, were calculated from 200 measurements. Cryo-electron microscopic analysis of the lipoprotein samples was performed as described by Van Antwerpen and Gilkey (10). Lipoprotein samples were stored at 4°C under nitrogen and in the presence of 10 μM Trolox for no more than a week before ultra-rapid freezing of the cryo-EM preparations. Shortly before freezing, lipoprotein solutions were diluted to a protein concentration of ca. 0.5 mg/ml in 150 mM NaCl, 5 mM EDTA, pH 7.0. Subsequently, a 4-μl lipoprotein sample was deposited on a 300-mesh electron microscope grid with a lacey substrate. Excess fluid was removed from the grid with Whatman No. 1 filter paper until thin aqueous films of the sample were formed in the holes of the lacey substrate. The sample was then plunge-frozen in liquid propane and stored in liquid nitrogen. Frozen hydrated samples were analyzed at 120 kV and at a temperature of −164°C, using a Philips EM 420 electron microscope (Philips, Eindhoven, The Netherlands) and a Gatan model 626 cryo transfer system (Gatan, Inc., Warrendale, PA). Photographs were taken at an instrumental magnification of 29,000 ×, and at ~2.4 μm underfocus. For each photographic recording, the electron dose was estimated to be ca. 1000 $e^{-} \cdot nm^{-2}$.

RESULTS

Negative staining

In negatively stained preparations, N-LDL (**Fig. 1A**) and PD-LDL (Fig. 1B) are seen as circular profiles with mean diameters of 26.4 ± 3.9 nm and 26.6 ± 3.9 nm, respectively. The micrographs demonstrate that the experimental removal of phospholipids from N-LDL had no detectable influence on the size or shape of the lipoprotein particles. Negatively stained SD-LDL particles have a mean diameter of 18.7 ± 0.9 nm (Fig. 1C). The observation that N-LDL, PD-LDL, and SD-LDL appear smaller in frozen hydrated preparations than in negatively stained preparations (see below) suggests that some flattening of the particles may have occurred during negative staining procedures. In Fig. 1D, discoidal rHDL particles are seen edge-on in typical rouleaux and face-on as round profiles. The rHDL particles are homogeneous discoidal complexes with a mean diameter of 18.8 ± 2.2 nm.

Cryo-electron microscopy

N-LDL. **Figure 2A** shows different projections of N-LDL in vitreous ice. Both rectangular projections with two high density bands and circular projections with a high density ring are recognized. (Selected rectangular and circular projections of N-LDL are shown in Fig. 6A.) Rectangular projections are 21.3 ± 1.5 nm long and 12.5 ± 1.1 nm wide; the circular projections have a mean diameter of 21.7 ± 1.4 nm. The width of the individual high density bands in rectangular projections of N-LDL is approximately 5 nm. The present cryo-electron micrographs of N-LDL are similar to those described earlier (10). As the frozen hydrated samples have not been stained, the different projections of N-LDL reflect the distribution of structural elements with a high mass density within the lipoprotein particle.

PD-LDL. The structural features of PD-LDL in vitreous ice (Fig. 2B) are very similar to the features of N-LDL (Fig. 2A). This is consistent with the observation that, in negatively stained samples, neither the size nor the morphology of N-LDL was altered by phospholipase treatment (see above). In Fig. 2B, both rectangular projections with two high density bands and circular projections with a high density ring are recognized. The rectangular projections are 20.3 ± 1.4 nm long and 12.5 ± 0.9 nm wide; the circular projections have a mean diameter of 19.9 ± 1.9 nm. Tilting of the PD-LDL preparation over a total angle of 90° converts circular projections with a high density ring to rectangular projections with two high density bands and vice versa (**Fig. 3,** particles 1–3). However, rectangular projections of PD-LDL that are oriented with their long axis perpendicular to the axis of tilt remain rectangular upon tilting (Fig. 3, particles 4 and 5). (Selected projections of PD-LDL are shown in Fig. 6B; these projections are indistinguishable from those of N-LDL (Fig. 6A), indicating that the contribution of phospholipid headgroups to the observed high density structure of N-LDL is minor.) As

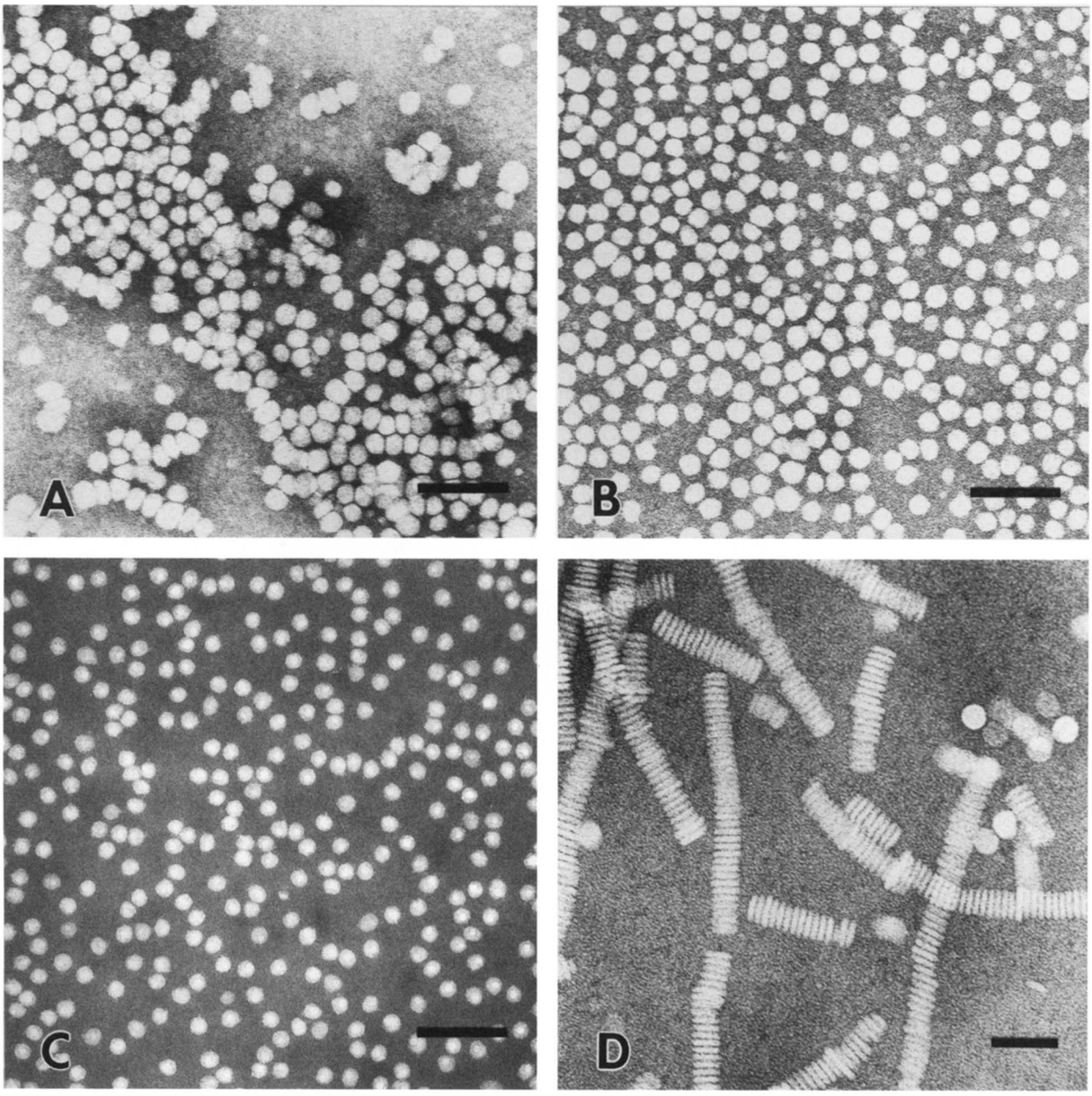

Fig. 1. Negative staining electron micrographs of N-LDL (A), PD-LDL (B), SD-LDL (C), and rHDL (D). Scale bars in A–C represent 100 nm. Scale bar in D represents 50 nm. The magnification of A–C is 136,000×; the magnification of D is 197,000×.

apoB is the only other high density component of N-LDL, the different projections of N-LDL and PD-LDL are indicated to reveal the distribution of apoB within the lipoprotein particle.

SD-LDL. Earlier studies have indicated that the conformation of apoB in SD-LDL differs from the conformation of apoB in N-LDL (8, 9). To determine whether this conformational difference can be detected using cryo-electron microscopy, we analyzed the structure of SD-LDL in vitreous ice. Figure 2C shows a typical cryo-electron micrograph of SD-LDL. No rectangular projections with two high density bands or circular projections with a high density ring are detected. Most projections of SD-LDL have an irregular shape. However, triangular and diamond-shaped projections are recognized frequently (see Fig. 6C). To determine whether these triangular and diamond-shaped projections can be obtained from a single particle, we recorded SD-LDL particles at +30° and −30° angles relative to the 0° plane of the goniometer (**Fig. 4**). In some cases, this tilting does convert triangular projections to diamond-shaped projections and vice versa (Fig. 4, particles 3, 5,

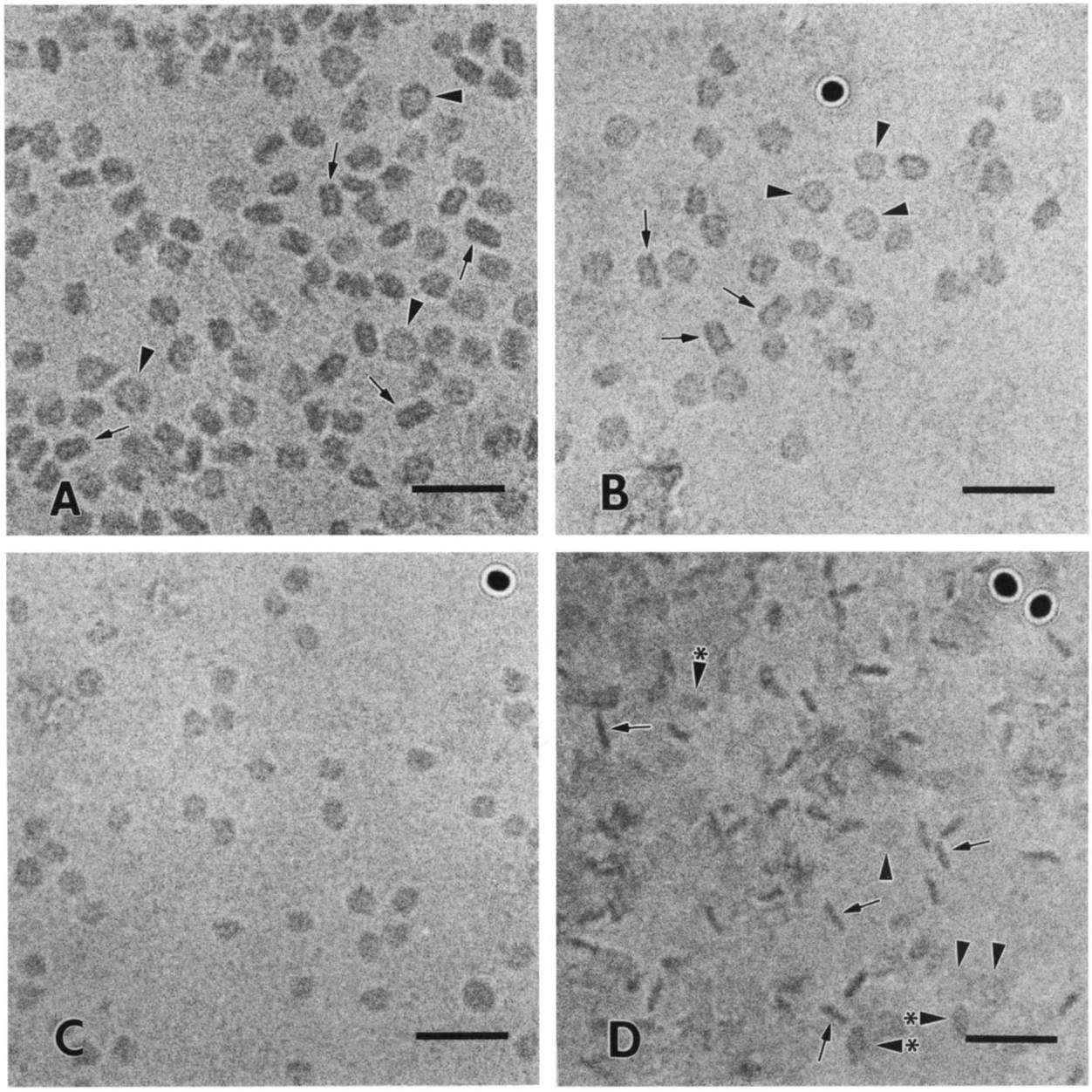

Fig. 2. A: Cryo-electron micrograph of N-LDL. Random orientation of the lipoproteins in vitreous ice results in different types of projections of the N-LDL particles. Both rectangular projections, with two parallel bands of high density (arrows) and circular projections with a ring of high density (arrowheads), can be recognized. B: Cryo-electron micrograph of PD-LDL. Projections of PD-LDL in vitreous ice are very similar to the projections of N-LDL (2A). Both rectangular projections with two high density bands (arrows) and circular projections with a high density ring (arrowheads) are recognized. C: Cryo-electron micrograph of SD-LDL. The typical rectangular and circular projections of N-LDL are not observed. D: Cryo-electron micrograph of rHDL. Both elongated projections with high contrast (arrows) and circular projections with low contrast (arrowheads) are recognized. Elliptical projections of rHDL, resulting from intermediate views of the particle, are visible with intermediate contrast (asterisks). Dark dots with a halo in B, C, and D are colloidal gold particles included in the preparation as a focusing aid. Scale bars represent 50 nm. Magnification 275,000×.

and 6), suggesting that the observed high density component may have a tetrahedral shape. Within this overall shape, isolated globular domains of high density are recognized (Fig. 4B, particles 2, 8, 9, and 10). The different projections of SD-LDL in vitreous ice have a small dimension of 16.8 ± 1.6 nm, and a large dimension of 18.2 ± 1.2 nm.

The absence of rectangular projections with two high density bands or circular projections with a high density ring, as well as the presence of new triangular and dia-

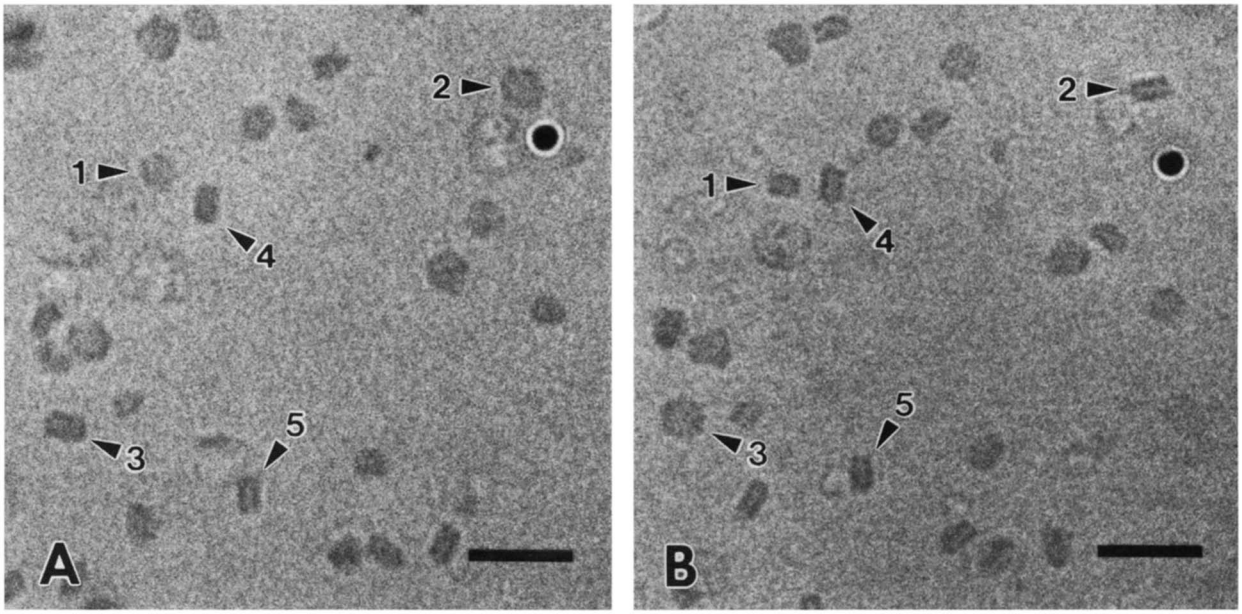

Fig. 3. Cryo-electron micrographs of PD-LDL, taken at +45° (A) and −45° (B) relative to the 0° plane of the goniometer. A and B are taken from the same area of the frozen hydrated preparation. Numbers indicate corresponding particles in the two micrographs. The tilt axis runs horizontally across the figure. Note how rectangular projections that are oriented with their long axis parallel to the axis of tilt are converted to circular projections with a high density ring upon tilting (particles 1, 2, and 3). However, rectangular projections that are oriented with their long axis perpendicular to the axis of tilt remain rectangular upon tilting (particles 4 and 5). The dark dot with the white halo is a colloidal gold particle, included in the preparation as a focusing aid. Scale bars represent 50 nm. Magnification 275,000×.

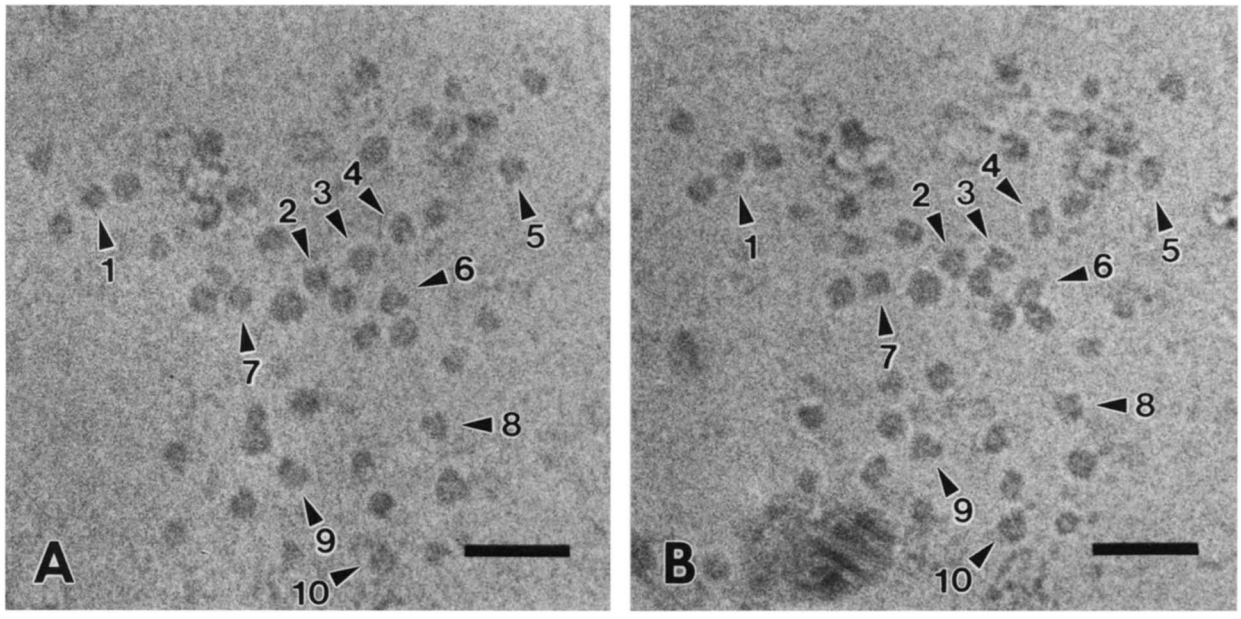

Fig. 4. Cryo-electron micrographs of SD-LDL, taken at +30° (A) and −30° (B) relative to the 0° plane of the goniometer. A and B are taken from the same area of the frozen hydrated preparation. Numbers indicate corresponding particles in the two micrographs. The tilt axis runs horizontally across the figure. Note how some of the triangular projections of the particle are converted to diamond-shaped projections upon tilting and vice versa (particles 3, 5, and 6). Scale bars represent 50 nm. Magnification 275,000×.

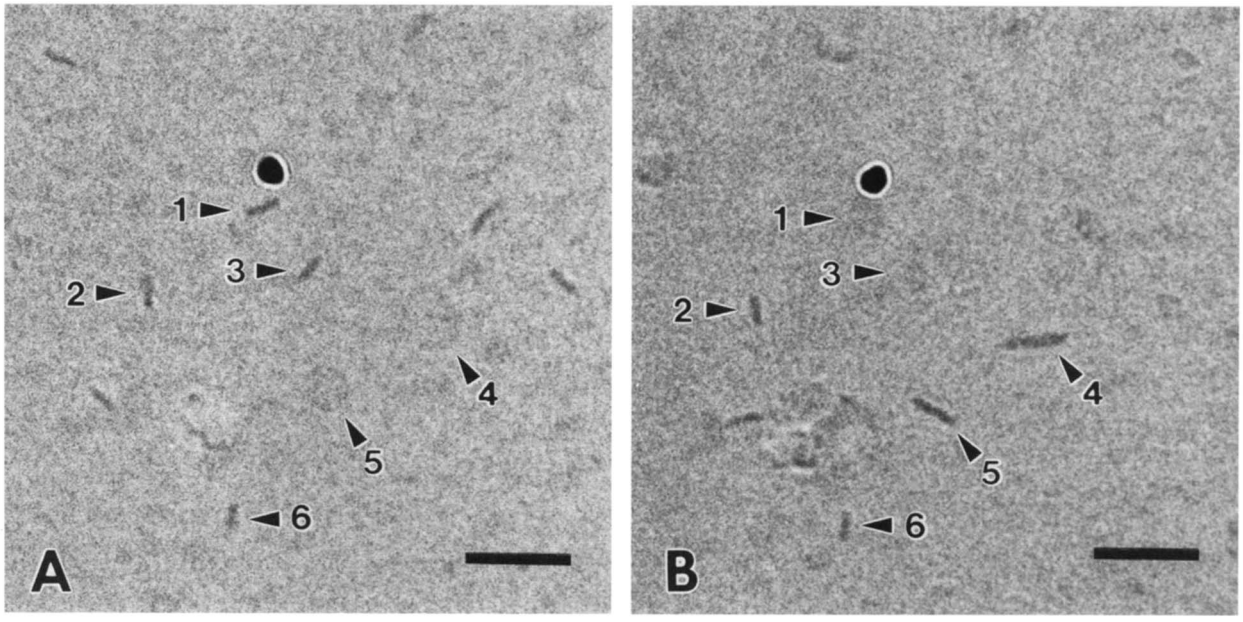

Fig. 5. Cryo-electron micrographs of rHDL, taken at +45° (A) and −45° (B) relative to the 0° plane of the goniometer. A and B are taken from the same area of the frozen hydrated preparation. Numbers indicate corresponding particles in the two micrographs. The tilt axis runs horizontally across the figure. Note how elongated projections that are oriented with their long axis roughly parallel to the axis of tilt are converted to circular projections upon tilting and vice versa (particles 1,3,4, and 5). However, elongated projections that are oriented with their long axis perpendicular to the tilt axis remain elongated upon tilting (particles 2 and 6). These observations are consistent with the discoid shape of the rHDL particles. The dark dot with the white halo is a colloidal gold particle, included in the preparation as a focusing aid. Scale bars represent 50 nm. Magnification 275,000×.

mond-shaped projections in preparations of SD-LDL, demonstrate that the high density structure in SD-LDL differs from the high density structure in N-LDL. This difference correlates with the putative conformational difference between the apoBs of SD-LDL and N-LDL (8, 9), and is consistent with the assertion that the observed high density structure represents apoB.

rHDL. To further test the hypothesis that cryo-electron microscopy visualizes the distribution of apolipoproteins, we analyzed rHDL particles, which are known to be phospholipid bilayer discs that are stabilized at the edge by apoA-1 (14, 15). Different types of projections of rHDL in vitreous ice are seen in Fig. 2D. The dimensions of these projections correspond with the dimensions of rHDL in negatively stained preparations (Fig. 1D), however, the characteristic rouleaux that are formed in negatively stained rHDL preparations are not seen in the frozen hydrated samples.

Edge-on views of discoidal rHDL particles produce ''elongated'' projections that are 18.8 ± 3.5 nm long and 5.1 ± 0.1 nm wide (Fig. 2D, **Fig. 5** and **Fig. 6D**). No structural features of the elongated projections correspond to either the dimensions or the presumed location of the phospholipid headgroups in rHDL [i.e., no parallel lines of high density separated by a more translucent space (cf. 12, 13) are observed]. Instead, the edge-on projections of rHDL consist of a single band of high density (Figs. 5 and 6D). The position of this high density band correlates with the putative location of the apoA-I molecules at the edge of the discoidal phospholipid bilayer (14, 15). Tilting of rHDL over an angle of 90° converts the elongated projections to circular projections and vice versa (Fig. 5). This is consistent with the discoidal shape of the complexes. The circular projections of rHDL have very low contrast (Figs. 2D, 5, and 6D) and are sometimes difficult to detect (Fig. 5, particles 1 and 3). However, a faint ring of elevated density around their periphery can frequently be observed (Fig. 5A, particles 4 and 5). The location of this ring-structure correlates with the putative location of apoA-I molecules at the edge of the rHDL disc (14, 15).

DISCUSSION

Cryo-electron microscopy permits the structural analysis of supra-molecular complexes in a fully hydrated state, without any form of chemical fixation or staining (24, 25). The technique is, therefore, thought to visualize biological samples very close to their native state. To date, many different molecular structures, including viruses (26–28), membrane proteins (29), and multisubunit enzyme complexes (30, 31) have been analyzed.

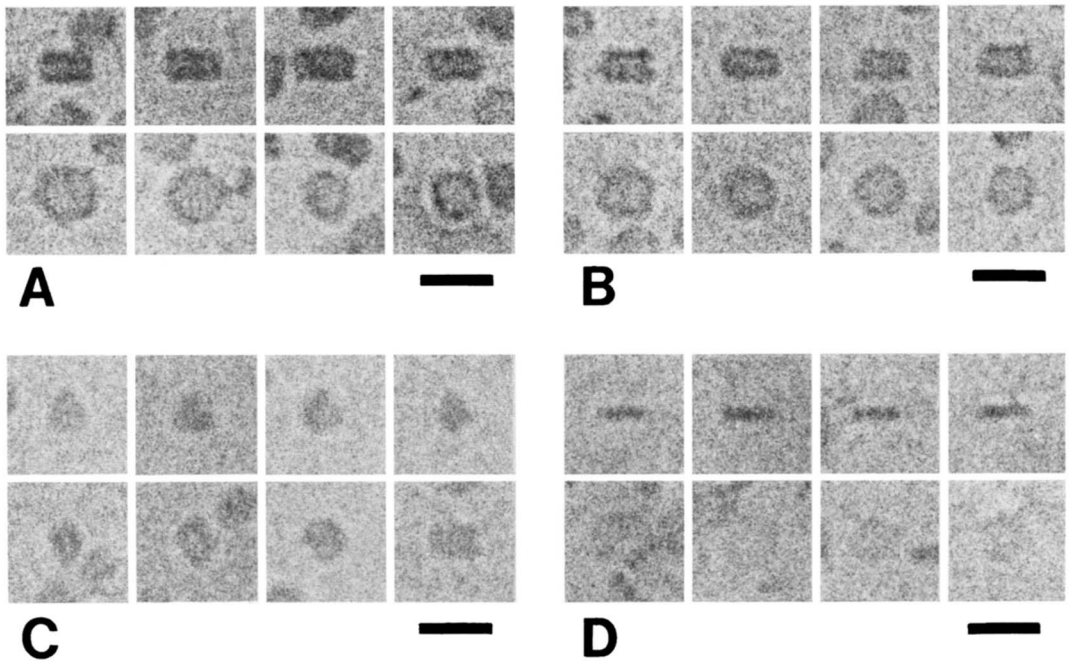

Fig. 6. Selected projections of N-LDL (A), PD-LDL (B), SD-LDL (C) and rHDL (D) in vitreous ice. A: Rectangular projections with two high density bands (top row) and circular projections with a high density ring (bottom row) of N-LDL. B: Rectangular projections with two high density bands (top row) and circular projections with a high density ring (bottom row) of PD-LDL. C: Triangular and diamond-shaped projections of SD-LDL. D: Elongated projections (top row) and circular projections (bottom row) of rHDL. Scale bars represent 25 nm. Magnification 375,000×.

Particularly noteworthy are recent studies on the structure of the *Escherichia coli* ribosome, in which cryo-electron microscopy has revealed the three-dimensional organization of high density ribosomal RNA relative to the lower density protein component of the particle (32, 33).

The contrast in a cryo-electron microscopic image correlates with differences in mass density within the microscopic preparation (34). Thus, a structural element with the same mass density as the solvent in which it is frozen will provide no contrast and will in effect be invisible in a cryo-electron micrograph of the preparation. However, when a structural element has a lower or higher mass density than the solvent, the element may be visible with negative or positive contrast, respectively. We can, therefore, predict that in cryo-electron micrographs of lipoprotein particles (frozen in physiological saline) the only elements with positive contrast may be apolipoproteins and phospholipid headgroups.

Recently, we have analyzed the structure of human LDL using cryo-electron microscopy (10). In this study, we have described typical projections of the lipoprotein particle that were either rectangular with two high density bands or circular with a high density ring. Tilting experiments demonstrated that the two types of projections can be obtained from a single particle, indicating that the observed high density component of LDL is organized as a double ring around the low density core of the particle. As apoB is the principal high density component of LDL (1), these data suggested that cryo-electron microscopy may visualize the distribution of apoB in LDL (10).

The present analysis of phospholipid-depleted N-LDL (PD-LDL) supports this suggestion. Although PD-LDL contains ca. 79% less phospholipid than N-LDL, different projections of PD-LDL in vitreous ice are virtually identical to those of N-LDL (Figs. 2A,B and 6A,B). Both rectangular projections with two high density bands and circular projections with a high density ring are recognized in PD-LDL preparations. This observation demonstrates that the contribution of high density phospholipid headgroups to the observed structure is minor. In addition, the results suggest that the overall distribution of apoB in PD-LDL is similar to the distribution of apoB in N-LDL. In other words, apoB of PD-LDL, like apoB of N-LDL, appears to be organized as a double ring around the core of the lipoprotein particle. It should be noted that these observations do not exclude the possibility that the conformation of apoB changes upon the removal of phospholipids from N-LDL. However, if such a conformational change takes place it does not seem to involve a major redistribution of apoB in LDL.

The suggested ring-structure of apoB in N-LDL is

consistent with several earlier studies on the structure of this lipoprotein. First, the translucent center that is visible in circular projections of frozen hydrated N-LDL (Figs. 2A and 6A) corresponds to the projected location of the low density core of cholesteryl esters and triacylglycerol (35–39). It has been suggested that apoB is in contact with this core, but the molecule is generally thought to be excluded from it (1). Furthermore, Phillips and Schumaker (5) have demonstrated that lipid extraction of N-LDL on electron microscope grids leaves a ring-shaped remnant that is thought to represent apoB. This remnant may well correspond to the high density ring-structure that is seen in the present study. Finally, the immuno-electron microscopic mapping of apoB epitopes on the surface of N-LDL indicates that apoB is organized in a "ribbon-and-bow" around the lipoprotein particle (6, 7). Although a bow structure is not resolved in the present study, the overall organization of high density in cryo-electron micrographs of N-LDL is in general agreement with the ribbon-and-bow model (7).

It has recently been suggested that a rectangular appearance of human LDL in vitreous ice may result from deformation (caused by either close packing of the particles or by surface tension forces present in the thin films of ice before freezing) and/or from oxidation (11). The present data, as well as earlier observations (10), do not support this suggestion. Our results demonstrate clearly that rectangular projections of N-LDL are observed in free-standing particles, excluding the possibility that the rectangular appearance of LDL is caused by a close packing of the particles. In addition, we have shown that rectangular projections are present in those areas of the preparation in which the vitreous ice is much thicker than the particles' diameter (10). This observation demonstrates that the rectangular appearance of LDL is not the result of a flattening by the surface tension forces in thin films of ice. Finally, our results show that a rectangular projection with two high density bands is converted to a circular projection with a high density ring when the N-LDL particle is tilted appropriately by 90° (10). The fact that both rectangular and circular projections can be obtained from a single particle demonstrates that the structural difference between rectangular and circular projections does not differentiate between oxidized and non-oxidized particles.

The assertion that cryo-electron microscopy visualizes the organization of apoB in LDL, is further supported by the analysis of SD-LDL. Earlier studies have indicated that the conformation of apoB in SD-LDL differs from the conformation of apoB in N-LDL. Compared to apoB in N-LDL, apoB in SD-LDL has a higher content of β-structure (8, 9) and an altered proteolytic accessibility (8). Furthermore, SD-LDL has a decreased affinity for the LDL-receptor of human fibroblasts (8, 9), which supports the suggestion that the conformation of apoB in this particle differs from the conformation of apoB in N-LDL. The putative conformational difference between the apoBs of N-LDL and SD-LDL correlates with the structural observations of the present study. In cryo-electron microscopic preparations of SD-LDL, rectangular projections with two high density bands and circular projections with a high density ring (the two typical projections of N-LDL) are rare. Instead, triangular and diamond-shaped projections of high density are detected. Frequently, these projections contain isolated domains of high density. These observations strongly suggest that the observed high density structure reflects the organization of apoB in LDL.

It should be noted that projections similar to those observed in preparations of SD-LDL are seen in preparations of N-LDL and PD-LDL. With regard to this observation, the following should be considered. When the "double-ring structure" seen in N-LDL and PD-LDL is not viewed edge-on or face-on but at some intermediate angle, the projected image may be characterized as "undefined" (10), and some of these undefined projections resemble projections of SD-LDL. However, the typical rectangular projections with two high density bands and the circular projections with a high density ring are not found at any angle of tilt in the present SD-LDL preparations. We can therefore conclude that the observed SD-LDL projections do not represent intermediate views of a double ring structure. As it is impossible to prove or disprove that all "undefined" projections of N-LDL are indeed intermediate views of a double ring structure, it cannot be fully excluded that N-LDL and PD-LDL preparations contain a subpopulation of particles whose structure resembles the structure of SD-LDL.

The analysis of discoidal rHDL in vitreous ice further confirms the hypothesis that cryo-electron microscopy visualizes the distribution of apolipoproteins in lipoprotein particles. In view of the above, rHDL is a particularly interesting particle, as the organization of phospholipids and apolipoproteins within the rHDL complex has been established (14, 15). The phospholipids of the particle form a flat, circular bilayer that is stabilized at the edge by apoA-I. The apoA-I molecules are thought to fully cover the hydrophobic acyl chains at the edge of the disc (14, 15). Hence, in face-on views of the particle, the apolipoprotein moiety is projected as a ring, while in edge-on views it is projected as a high density "band" with dimensions that roughly correspond to the diameter and the thickness of the phospholipid bilayer.

The circular projections of rHDL in vitreous ice have very low contrast relative to the background of frozen

saline. Especially, the central areas of circular projections (which contain phospholipids and cholesterol, but no apolipoproteins) are depicted with low contrast. This demonstrates that the phospholipid molecules, at least in this orientation (i.e., with their long axes parallel to the electron beam) are almost invisible in the cryo-electron microscopic image of the rHDL particle. Frequently, however, circular projections with a ring of elevated density around their perimeter can be detected (see Fig. 5A, particles 4 and 5). The location of this ring-structure correlates with the location of apoA-I, molecules on the periphery of the lipoprotein disc, indicating that in those particular projections the apolipoprotein moiety of rHDL is visualized.

Contrary to the circular projections, the elongated projections of rHDL have a high contrast relative to the background (Figs. 5 and 6D). Within the high density band of elongated projections, the two projected lines of phospholipid headgroups (outlining the "top" and the "bottom" of the elongated projection) are not resolved. Instead, a solid band of high density is detected, and this high density structure correlates with the putative location of apoA-I molecules at the edge of the phospholipid bilayer.

The tilting experiment of Fig. 5 demonstrates that the contrast of an elongated projection of rHDL is much higher than the contrast of a circular projection of the particle. A possible explanation for this difference in contrast may be that, in perfect face-on views of the rHDL disc, the projected ring-structure of the apolipoprotein moiety is only as wide as the diameter of the amphipathic α-helixes of apoA-I (14, 15). Hence, the ring-structure may not easily be resolved in circular projections of the particle.

Taken together, the present results show that *1*) the removal of phospholipids from N-LDL has no major influence on the contrast of the high density structure that is seen in cryo-electron micrographs of the particle, indicating that the contribution of phospholipid headgroups to the observed structure is minor; *2*) the high density structures seen in cryo-electron micrographs of N-LDL and SD-LDL are different, and this difference correlates with the conformational difference that is thought to exist between the apoBs of N-LDL and SD-LDL; and *3*) the distribution of high density in cryo-electron micrographs of rHDL correlates with the location of apolipoprotein A-I molecules on the periphery of the phospholipid bilayer disc. These observations strongly indicate that cryo-electron microscopy visualizes the distribution of apolipoproteins in lipoprotein particles.

We wish to thank Dr. Verne Schumaker for stimulating discussions, Laura Knoff for her excellent technical assistance, and David Bentley from the Imaging Facilities, Division of Biotechnology (ARL), at the University of Arizona for providing laboratory space and equipment to perform the cryo-electron microscopy. This work was supported by the National Institutes of Health Grant GM50551 (to RVA), by the National Institutes of Health Grant HL 14237 (Arteriosclerosis Specialized Center of Research), and by the National Institutes of Health Program Project Grant HL 18574 from the National Heart, Lung, and Blood Institute. Work at the Ernest Orlando Lawrence Berkeley National Laboratory was conducted through the U.S. Department of Energy under Contract No. DE-AC03-76SF00098. CRP is the recipient of a grant from the Joseph Drown Foundation.

Manuscript received 25 July 1996 and in revised form 23 December 1996.

REFERENCES

1. Schumaker, V. E., M. L. Phillips, and J. E. Chatterton. 1994. Apolipoprotein B and low density lipoprotein structure: implications for biosynthesis of triglyceride-rich lipoproteins. *Adv. Prot. Chem.* **45:** 205–248.
2. Knott, T. J., R. J. Pease, L. M. Powell, S. C. Wallis, S. C. Rall, T. L. Innerarity, B. Blackhart, W. H. Taylor, Y. Marcel, R. Milne, D. Johnson, M. Fuller, A. J. Lusis, B. J. McCarthy, R. W. Mahley, B. Levy-Wilson, and J. Scott. 1986. Complete protein sequence and identification of structural domains of human apolipoprotein B. *Nature.* **323:** 734–738.
3. Yang, C-Y., S-H. Chen, S. H. Gianturco, W. A. Bradley, J. T. Sparrow, M. Tanimura, W-H. Li, D. A. Sparrow, H. DeLoof, M. Rosseneu, F-S. Lee, Z-W. Gu, A. M. Gotto, Jr., and L. Chan. 1986. Sequence, structure, receptor-binding domains and internal repeats of human apolipoprotein B-100. *Nature.* **323:** 738–742.
4. Chan, L. 1992. Apolipoprotein B, the major protein component of triglyceride-rich and low density lipoproteins. *J. Biol. Chem.* **267:** 25621–25624.
5. Phillips, M. L., and V. N. Schumaker. 1989. Conformation of apolipoprotein B after lipid extraction of low density lipoproteins attached to an electron microscope grid. *J. Lipid Res.* **30:** 415–422.
6. Chatterton, J. E., M. L. Phillips, L. K. Curtiss, R. W. Milne, Y. L. Marcel, and V. N. Schumaker. 1991. Mapping apolipoprotein B on the low density lipoprotein surface by immunoelectron microscopy. *J. Biol. Chem.* **266:** 5955–5962.
7. Chatterton, J. E., M. L. Phillips, L. K. Curtiss, R. Milne, J-C. Fruchart, and V. N. Schumaker. 1995. Immunoelectron microscopy of low density lipoproteins yields a ribbon and bow model for the conformation of apoB on the lipoprotein surface. *J. Lipid Res.* **36:** 2027–2037.
8. Chen, G. C., W. Liu, P. Duchateau, J. Allaart, R. L. Hamilton, C. M. Mendel, K. Lau, D. A. Hardman, P. H. Frost, M. J. Malloy, and J. P. Kane. 1994. Conformational differences in human apolipoprotein B-100 among subspecies of low density lipoproteins (LDL). Association of altered proteolytic accessibility with decreased receptor binding of LDL subspecies from hypertriglyceridemic subjects. *J. Biol. Chem.* **269:** 29121–29128.
9. Galeano, N. F., R. Milne, Y. L. Marcel, M. T. Walsh, E. Levy, T. D. Ngu'yen, A. Gleeson, Y. Arad, L. Witte, M. Al-Haideri, S. C. Rumsey, and R. J. Deckelbaum. 1994. Apo-

protein B structure and receptor recognition of triglyceride-rich low density lipoprotein (LDL) is modified in small LDL but not in triglyceride-rich LDL of normal size. *J. Biol. Chem.* **269:** 511–519.
10. Van Antwerpen, R., and J. C. Gilkey. 1994. Cryo-electron microscopy reveals human low density lipoprotein substructure. *J. Lipid Res.* **35:** 2223–2231.
11. Spin, J. M., and D. Atkinson. 1995. Cryo-electron microscopy of low density lipoprotein in vitreous ice. *Biophys. J.* **68:** 2115–2123.
12. Lepault, J., F. Pattus, and N. Martin. 1985. Cryo-electron microscopy of artificial biological membranes. *Biochim. Biophys. Acta.* **820:** 315–318.
13. Dubochet, J., M. Adrian, J. Lepault, and A. D. McDowall. 1985. Cryo-electron microscopy of vitrified biological specimens. *Trends Biochem. Sci.* **10:** 143–146.
14. Atkinson, D., and D. M. Small. 1986. Recombinant lipoproteins: implications for structure and assembly of native lipoproteins. *Annu. Rev. Biophys. Biophys. Chem.* **15:** 403–456.
15. Jonas, A. 1992. Lipid-binding properties of apolipoproteins. *In* Structure and Function of Apolipoproteins. M. Rosseneu, editor. CRC Press, Boca Raton, FL. 217–250.
16. Lindgren, F. T., L. C. Jensen, and F. T. Hatch. 1972. The isolation and quantitative analysis of serum lipoproteins. *In* Blood Lipids and Lipoproteins: Quantitation, Composition, and Metabolism. G. J. Nelson, editor. John Wiley and Sons, New York. 181–274.
17. Bartlett, G. R. 1959. Phosphorus assay in column chromatography. *J. Biol. Chem.* **234:** 466–471.
18. Nichols, A. V., E. L. Gong, P. J. Blanch, and T. M. Forte. 1983. Characterization of discoidal complexes of phosphatidylcholine, apoA-I, and cholesterol by GGE. *Biochim. Biophys. Acta.* **750:** 353–364.
19. Matz, C. E., and A. Jonas. 1982. Reaction of human lecithin:cholesterol acyltransferase with synthetic micellar complexes of apolipoprotein A-I, phosphatidylcholine, and cholesterol. *J. Biol. Chem.* **257:** 4541–4546.
20. Swaney, J. B., and K. O'Brien. 1978. Cross-linking studies of the self-associated properties of apoA-I and apoA-II from human high density lipoprotein. *J. Biol. Chem.* **253:** 7069–7077.
21. Nichols, A. V., P. J. Blanche, and E. L. Gong. 1983. Gradient gel electrophoresis of human plasma high density lipoproteins. *In* CRC Handbook of Electrophoresis. Vol. III. L. Lewis and J. Opplt, editors. CRC Press, Boca Raton, FL. 29–47.
22. Markwell, M. A. K., S. M. Hass, L. L. Bieber, and N. E. Tolbert. 1978. A modification of the Lowry procedure to simplify protein determination in membrane and lipoprotein samples. *Anal. Biochem.* **87:** 206–210.
23. Forte, T. M., and R. W. Nordhausen. 1986. Electron microscopy of negatively stained lipoproteins. *Methods Enzymol.* **128:** 442–457.
24. Dubochet, J., M. Adrian, J-J. Chang, J-C. Homo, J. Lepault, A. W. McDowall, and P. Schulz. 1987. Cryo-electron microscopy of vitrified specimens. *Q. Rev. Biophys.* **21:** 129–228.
25. Adrian, M., J. Dubochet, J. Lepault, and A. W. McDowall. 1984. Cryo-electron microscopy of viruses. *Nature.* **308:** 32–36.
26. Vogel, R. H., S. W. Provencher, C-H. von Bonsdorff, M. Adrian, and J. Dubochet. 1986. Envelope structure of Semliki Forest virus, reconstructed from cryo-electron micrographs. *Nature.* **320:** 533–535.
27. Baker, T. S., W. W. Newcomb, N. H. Olson, L. M. Cowsert, C. Olson, and J. C. Brown. 1991. Structures of bovine and human papillomaviruses. Analysis by cryoelectron microscopy and three-dimensional image reconstruction. *Biophys. J.* **60:** 1445–1456.
28. Paredes, A. M., D. T. Brown, R. Rothnagel, W. Chiu, R. J. Schoepp, R. E. Johnston, and B. V .V. Prasad. 1993. Three-dimensional structure of a membrane-containing virus. *Proc. Natl. Acad. Sci. USA.* **90:** 9095–9099.
29. Toyoshima, C., H. Sasabe, and D. L. Stokes. 1993. Three-dimensional cryo-electron microscopy of the calcium ion pump in the sarcoplasmic reticulum membrane. *Nature.* **362:** 469–471.
30. Wagenknecht, T., R. Grassucci, and D. Schaak. 1990. Cryo-electron microscopy of frozen-hydrated α-ketoacid dehydrogenase complexes from *Escherichia coli*. *J. Biol. Chem.* **265:** 22402–22408.
31. Wagenknecht, T., R. Grassucci, G. A. Radke, and T. E. Roche. 1991. Cryo-electron microscopy of mammalian pyruvate dehydrogenase complex. *J. Biol. Chem.* **266:** 24650–24656.
32. Frank, J., J. Zhu, P. Penczek, Y. Li, S. Srivastava, A. Verschoor, M. Rademacher, R. Grassucci, R. K. Lata, and R. K. Agrawal. 1995. A model of protein synthesis based on cryo-electron microscopy of the *E. coli* ribosome. *Nature.* **376:** 441–444.
33. Stark, H., F. Mueller, E. V. Orlova, M. Schatz, P. Dube, T. Erdemir, F. Zemlin, R. Brimacombe, and M. van Heel. 1995. The 70S *Escherichia coli* ribosome at 23 Å resolution: fitting the ribosomal RNA. *Structure.* **3:** 815–821.
34. Lepault, J., F. P. Booy, and J. Dubochet. 1983. Electron microscopy of frozen biological suspensions. *J. Microsc.* **129:** 89–102.
35. Müller, K., P. Laggner, O. Glatter, and G. Kostner. 1978. The structure of human plasma low density lipoprotein B. An X-ray small-angle scattering study. *Eur. J. Biochem.* **82:** 73–90.
36. Deckelbaum, R. J., G. G. Shipley, and D. M. Small. 1977. Structure and interactions of lipids in human plasma low density lipoproteins. *J. Biol. Chem.* **252:** 744–754.
37. Atkinson, D., R. J. Deckelbaum, D. M. Small, and G. G. Shipley. 1977. Structure of human plasma low density lipoproteins: molecular organization of the central core. *Proc. Natl. Acad. Sci. USA.* **74:** 1042–1046.
38. Luzatti, V., A Tardieu, and L. P. Aggerbeck. 1979. Structure of serum low-density lipoprotein. I. A solution X-ray scattering study of a hyperlipidemic monkey low-density lipoprotein. *J. Mol. Biol.* **131:** 435–473.
39. Laggner, P., G. M. Kostner, G. Degovics, and D. L. Worcester. 1984. Structure of the cholesterol ester core of human plasma low density lipoproteins: selective deuteration and neutron small-angle scattering. *Proc. Natl. Acad. Sci. USA.* **81:** 4389–4393.